TURBULENCE IN CIRRUS CLOUDS – IMPACT OF CRITICAL LAYERS

Peter Spichtinger[1]*, **and Piotr K. Smolarkiewicz**[2]

[1] ETH Zurich, Institute for Atmospheric and Climate Science, Zurich, Switzerland
[2] National Center for Atmospheric Research, Boulder, Colorado, USA

We investigate the impact of gravity-wave induced turbulence in critical layers on the formation and evolution of cirrus clouds in ice-supersaturated regions. The anelastic non-hydrostatic computational model EULAG (http://www.mmm.ucar.edu/eulag) employs a recently developed ice microphysics scheme. An idealized framework includes time-dependent lower boundary for excitation of waves with prescribed wave number and amplitude, and arbitrarily specified ice–supersaturated layer in the vicinity of the critical level. The formation of ice crystals triggered by the laminar wave motion and turbulence in critical layer aloft are both captured in the simulation.

1 INTRODUCTION

Clouds are still one of the least understood components of the climate system. As stated in the IPCC report (IPCC, 2007) and during the recent international workshop at the Ernst Strüngmann Forum (http://fias.uni-frankfurt.de/esforum/clouds.html), cloud properties and their impact on the radiation budget in changing climate are not sufficiently known. Especially, the impact of high clouds consisting purely of ice crystals, viz. cirrus clouds, is known poorly, although a net warming is typically assumed (Chen et al., 2000). However, recent studies of the radiative properties of mid latitude cirrus clouds indicate that under certain conditions the transition between warming (i.e., for dominating absorption of thermal radiation) and cooling (i.e., for dominating reflection of solar radiation) strongly depends on the ice crystal number concentration, whereas the ice water content determines mainly the magnitude of warming or cooling (Fusina et al., 2007).

Generally, there are two distinct processes of ice crystal formation in the upper troposphere (Vali, 1985): a homogeneous freezing of aqueous solution droplets (Koop et al., 2000) or heterogeneous nucleation on aerosol particles — so-called ice nuclei, hereafter IN for brevity — (DeMott et al., 2003). At high temperatures ($T > 235$ K) ice crystals are formed via heterogeneous nucleation, whereas in the low temperature range ($T < 235$ K) homogeneous freezing is the dominant pathway (Kärcher and Ström, 2003); yet heterogeneous IN can modify homogeneous nucleation (Kärcher et al., 2006; Spichtinger and Gierens, 2008b). Homogeneous nucleation depends strongly on vertical velocity and temperature (Kärcher and Lohmann, 2002; Spichtinger and Gierens, 2008a). Variations of the updraft velocity inducing adiabatic cooling can easily effect in a few orders of magnitude change in the ice crystal concentration number. In consequence, these variations of vertical velocity have strong impact on radiative properties of the resulting cirrus clouds.

Although cirrus clouds appear quite homo-

*peter.spichtinger@env.ethz.ch

geneous from a satellite perspective (e.g., a warm-front cirrus), even a casual glance from the ground reveals an inhomogeneous, patchy structure of cirrus. Furthermore, in situ measurements (Schlicht et al., 2006; Gayet et al., 2004; Krämer, 2008) document that cirrus clouds have high internal variability. Inside cirrus, temperature and vertical velocity fluctuations are substantial, thus causing inhomogeneities in ice crystal number concentration and ice water content. Based on temperature and/or vertical velocity measurements in the upper troposphere (e.g. Gary, 2006; Gierens et al., 2007) an "ubiquitous" background of temperature fluctuations is often assumed. This feature is typically used for a random offset of box-model calculations of ice crystal formation in large-scale motions (Haag and Kärcher, 2004; Hoyle et al., 2005). However, these fluctuations (of temperature and/or vertical velocity) have a deterministic physical origin. In particular, small-scale variations can be related to turbulence generated by breaking internal gravity waves. Notably, measurements indicate that in the tropopause region, where cirrus clouds occur preferentially, turbulence is found frequently (Smith and Jonas, 1996; Worthington, 1999). One plausible source for turbulence are nonlinear interactions of orographic waves with sheared ambient wind within critical layers (Booker and Bretherton, 1967; Worthington and Thomas, 1996). As the gravity wave approaches the critical level, it becomes increasingly shorter, overturns and breaks; thus generating turbulence and mixing (Grubisic and Smolarkiewicz, 1997).

Herein, we study the impact of turbulence generated in critical layers on the formation and evolution of ice–supersaturated regions (i.e., latent regions of cirrus formation) and cirrus clouds. Our primarily tool of research is the anelastic nonhydrostatic computational model EULAG (Smolarkiewicz and Margolin, 1997; Prusa et al. 2008) combined with a recently developed ice microphysics scheme (Spichtinger and Gierens, 2008a). The vertically propagating wave and the associated critical layer effects are simulated using an idealized scenario.

In the next section, the computational model and ice microphysics scheme are briefly described. In section 3 the model setup and parameters of sensitivity studies are specified. In section 4 the simulation results are summarized, while section 5 concludes the paper.

2 MODEL DESCRIPTION

2.1 DYNAMICAL MODEL DESCRIPTION

The multiscale dynamic model EULAG has been broadly documented in the literature; see Prusa et al. 2008, for a recent review. For dry dynamics, the anelastic equations employed in the present study can be written in perturbation form as follows (cf. Smolarkiewicz et al., 2001)

$$\nabla \cdot \bar{\rho}\mathbf{u} = 0 \quad (1)$$

$$\frac{D\mathbf{u}}{Dt} = -\nabla\left(\frac{p'}{\bar{\rho}}\right) - \mathbf{g}\left(\frac{\theta'}{\bar{\theta}}\right) - \mathbf{f}\times\mathbf{u}' \quad (2)$$

$$\frac{D\theta'}{Dt} = -\mathbf{u}\cdot\nabla\theta_e \quad (3)$$

Here, $\mathbf{u}$ is the velocity vector; p, ρ and θ denote pressure, density and potential temperature, respectively; **g** and **f** denote vectors of, respectively, gravitational acceleration and Coriolis parameter; $\bar{\theta}$ and $\bar{\rho}$ are the anelastic reference-state profiles for potential temperature and density. The subscript $_e$ refers to balanced ambient profiles, not necessarily equal to the profiles of the reference state; cf. Smolarkiewicz et al., 2001 for a discussion. Primes denote deviations from the environmental state (e.g. $\theta' = \theta - \theta_e$), and $\frac{D}{Dt} := \partial/\partial t + \mathbf{u}\cdot\nabla$ is the total derivative.

The approximate solutions of the prognostic equations (2) and (3) are evaluated using the unified semi-Lagrangian/Eulerian approach broadly described in the literature (see Prusa et al. 2008 and the references therein). Let $\mathbf{\Psi}$ and $\mathbf{F}$ denote, respectively, the vectors of dependent variables (u, v, w, θ') and their associated forcings. With $\tilde{\mathbf{\Psi}} := \mathbf{\Psi}^n + 0.5\Delta t\mathbf{F}^n$ and the generalized forward-in-time non-oscillatory transport operator LE, the approximate solu-

tion can be compactly written as

$$\mathbf{\Psi}_{\mathbf{i}}^{n+1} = LE_{\mathbf{i}}\left(\tilde{\mathbf{\Psi}}\right) + 0.5\Delta t\mathbf{F}_{\mathbf{i}}^{n+1} \qquad (4)$$

whereby $\mathbf{i}$ and n denote, respectively, spatial and temporal location on the mesh. The forcing $\mathbf{F}^{n+1} = \mathbf{F}(\mathbf{\Psi}^{n+1})$, thus implying the trapezoidal-rule (implicit) integration of the governing equations. Inverting the implicit formulae (4) involves formulation and solution of the elaborate elliptic equation for the pressure perturbation, implied by the mass continuity in (1). For extensions to moist thermodynamics see Grabowski and Smolarkiewicz (2002).

The model outlined was used in many applications on different scales and for disperse problems of geophysical fluid dynamics (in particular, for stratified orographic flows and convectively generated gravity waves pertinent to this study). One noteworthy aspect of EULAG is its design around the non-oscillatory advection scheme MPDATA (for multidimensional positive definite advection transport algorithm; see Smolarkiewicz, 2006, for a recent overview).

2.2 ICE MICROPHYSICS DESCRIPTION

Here, we provide a brief overview of the parameterized microphysical processes employed in this study. For a detailed description the interested reader is referred to Spichtinger and Gierens (2008a).

A double-moment bulk microphysics scheme is utilized; i.e., prognostic equations are solved for ice crystal number and mass concentrations. Ice crystal mass (or equivalently size) is assumed to follow a lognormal distributions with time-dependent mean mass but fixed spectral width. Crystal shapes are droxtals (aspect ratio one) up to a diameter of 7.42 μm and columns with size–dependent aspect ratio for larger sizes. An arbitrary number of ice classes can be treated with this scheme. Each ice class is explicitly tied to an aerosol type that nucleates it, hence ice classes are distinguished by their formation mechanism (e.g., heterogeneously vs. homogeneously formed ice). The aerosol types are also characterized by their number and mass concentration.

The three microphysical processes parameterized to simulate cold cirrus are nucleation (homogeneous and heterogeneous), diffusional growth/evaporation and sedimentation. Ice crystal aggregation is neglected, because it is of minor importance for thermodynamics of cold cirrus ($T < 235$ K) as well as for the low vertical and terminal velocities (Kajikawa and Heymsfield, 1989) considered in our study.

For the representation of homogeneous freezing of aqueous solution droplets we prescribe lognormally-distributed sulfuric acid drops as a background aerosol. The water content of the solution droplets is computed using the Koehler theory. Freezing rates are calculated using the water activity based and temperature dependent parameterization of Koop et al. (2000). In this study we focus on the homogeneous nucleation. The heterogeneous nucleation is not addressed, although parameterizations for these formation mechanisms are available in the model (Spichtinger and Gierens, 2008b). For parameterizing the diffusional growth of ice crystals, we use a modified Koenig ansatz (Koenig, 1971) with corrections for small crystals (i.e., droxtals) and ventilation. This approach for single ice crystals was extend to the bulk quantity (the cloud ice mixing ratio). For the evaporation of ice crystals, both the ice mass concentration and number concentration decrease in relative proportion, as described in (Spichtinger and Gierens, 2008a, sec. 3.3). To simulate sedimentation we use mass and number weighted terminal velocities, respectively, with parameterizations for single crystals adopted from Heymsfield and Iaquinta (2000).

3 EXPERIMENTAL SETUP

Our idealized framework assumes a 2D domain in the xz vertical plane, with periodic boundary conditions in the x direction. The horizontal and vertical extent of the domain are $L_x = 10$ km and $L_z = 15$ km, respectively. The model domain is discretized with $n_x \times n_z = 224 \times 335$ grid points, thus resulting in grid resolution $dx \approx$

44.8 m and $dz \approx 44.9$ m, in the horizontal and the vertical, respectively.

In order to excite waves with prescribed wave number and amplitude we specify: i) the constant-stratification ambient profile of potential temperature (Clark and Farley, 1984) with surface value $\theta_s = T_s = 288.18$ K and Brunt-Väisälä frequency $N = 0.0097\mathrm{s}^{-1}$; and ii) the linear wind profile with the surface value $u_0 = 10\,\mathrm{m\,s}^{-1}$ and constant shear of $du/dz = -10^{-3}\mathrm{s}^{-1}$; fig. 1. Furthermore, we specify a single Fourier mode for the lower boundary profile

$$z_b(t,x) = a(t) \cdot \sin\left(\frac{2\pi x}{x_0}\right) \tag{5}$$

with $x_0 = 10$ km and the time dependent amplitude

$$a(t) = \begin{cases} a_0 \cdot t/t_0 & \text{for} \quad t \le t_0 \\ a_0 & \text{for} \quad t > t_0 \end{cases} \tag{6}$$

with $t_0 = 405$ min. All simulations are for total time of $T_s = 720$ min, using temporal increment $dt = 2.5$ s. For the microphysics, we use a smaller time increment of $dt_{mp} = 0.25$ for vertical columns, only if homogeneous nucleation takes place somewhere in the column. Initial condition consists of the ambient wind and a Gaussian noise with standard deviation $\sigma_T = 0.1$ K for the perturbation potential temperature. Furthermore, a deep layer of ice supersaturation is specified in the altitude range $6 \le z \le 10$ km. As shown in fig. 1, this range is in the cold temperature regime ($T < 240$ K), so the cirrus may form by homogeneous nucleation.

4 RESULTS

The aim the simulation performed is to elucidate the overall impact of waves and turbulence occurring in critical layers on the moisture field and eventual ice crystal formation.

Figure 2 shows the time evolution of the vertical velocity in time intervals of 90 min, starting at 180 min. The time dependent lower boundary slowly forces the development of the orographic like gravity wave. The wave packet propagates in the vertical, and as it approaches the critical level at $z = 10$ km, the vertical component of the group velocity and the vertical wavelength tend to zero. The wave packet cannot reach the critical level, and is absorbed by the mean flow. The wave dissipates within the turbulent critical layer beneath $z_c = 10$ km. The corresponding fig. 3 illustrates the impact of waves and turbulence on the evolution of the moisture field and formation of ice crystals.

As the wave approaches the critical level, the associated updrafts and downdrafts cool down and warm up the environment adiabatically; thus correspondingly increasing/decreasing the initially prescribed supersaturation, depending on the position in the layer relative to the propagating wave. As the wave is developing, the supersaturation is increased in some regions, such that the thresholds for homogeneous nucleation are surpassed, and the ice crystals are formed. The cloud formation starts at the lower levels, due to the interplay of two distinct phenomena. First, because of the proximity to the forcing region, the magnitude of vertical velocity increases (chronologically) earlier

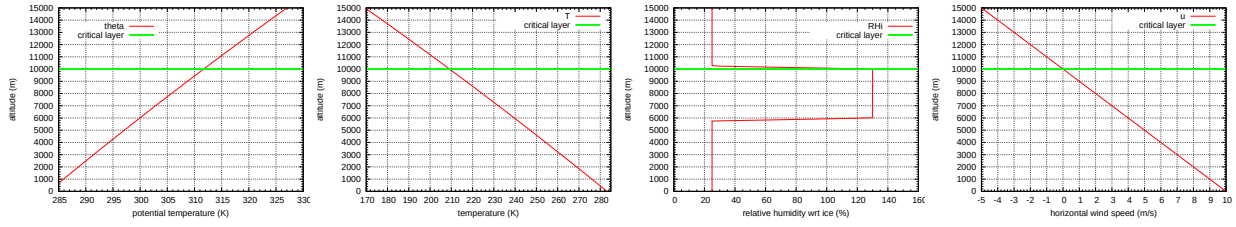

Fig. 1: Initial profiles for the idealized simulations. From left to right: potential temperature, temperature, relative humidity wrt ice and horizontal wind speed (red line). The theoretical position of the critical level (i.e., z at which $u = 0\,\mathrm{m\,s}^{-1}$) is indicated by the green line.

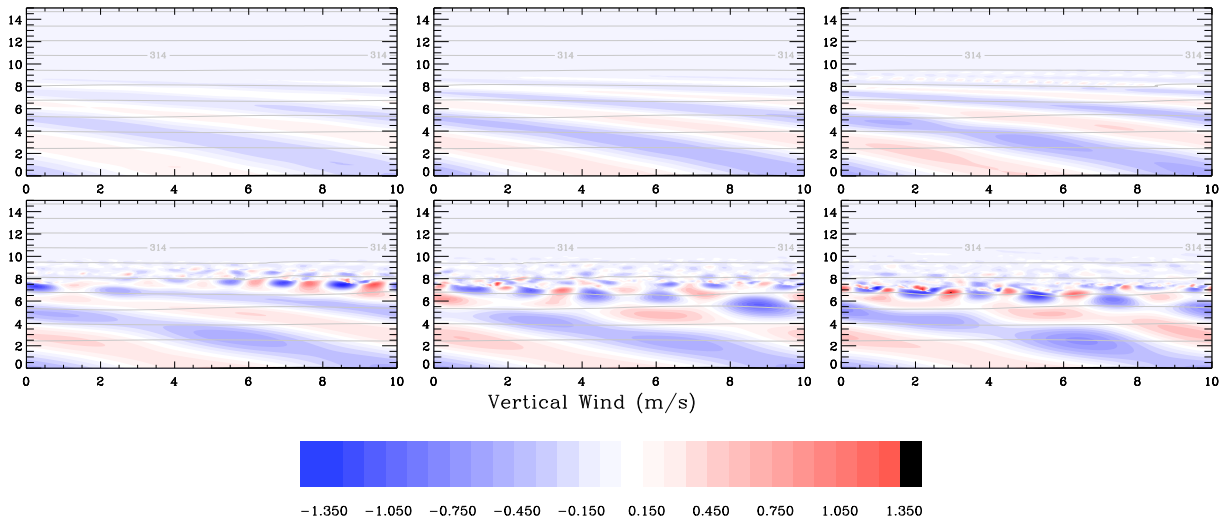

Fig. 2: Evolution of the vertical velocity forming a critical layer (time lag = 30 min), starting at simulation time $t_s = 270$ min (time lag = 90 min; upper panel:270/360/450 min, lower panel: 540/630/720 min). Grey lines indicate potential temperature.

in the lower part of the supersaturated layer. Second, the homogeneous nucleation thresholds (for different sizes of the aqueous solution droplets) are temperature dependent (Koop et al., 2000), such that the threshold for a fixed aerosol size increases with decreasing temperature. Hence, for the lower part of the supersaturation layer, nucleation can be triggered at lower thresholds; only a small uplift suffices to produce enough supersaturation for ice formation. In effect of the two mechanisms described, ice crystals form first in the lower part of the supersaturated layer, and subsequently the cirrus grows upward.

With the onset of turbulence near critical level, the vertical motions develop much stronger than in the laminar wave motion below. The larger updrafts can additionally trigger ice formation. However, the formation of ice crystals by the turbulent portion of the vertical velocity spectrum appears limited by some factors:

- In turbulent regions the spatial (and thus temporal) scale of updrafts is much smaller than in the laminar region below. For the ice crystal formation, the updrafts must be appreciated for some time, because ice supersaturation has to surpass the homogeneous nucleation thresholds and maintain the excess until a reasonable amount of ice crystals are formed.
- Here, the strongest updrafts driven by turbulence occur in the lower half of the ice supersaturated layer. However, depending on the environmental temperature and humidity, ice formation can be triggered by the wave motion even before the onset of the turbulence. In such a case, due to their diffusional growth, ice crystals act as a strong sink for the water vapor, thus reducing the local supersaturation. Moreover, as crystals reach adequate size, they fall out, and a local dehydration takes place. Hence, the eventual homogeneous nucleation in subsequent turbulent motions starts at lower supersaturation, thus reducing the ability to form ice crystals.

Figure 4 shows the probability density functions for the vertical velocity and the relative humidity, respectively, inside the layer ($4 \leq z \leq 10.5$ km). Here, a data point is labeled as cloudy if the ice crystal number density is larger than $0.1\mathrm{L}^{-1}$.

The vertical velocity spectrum is dominated by the small scale variations in the early time of the evolution, when the wave has not been

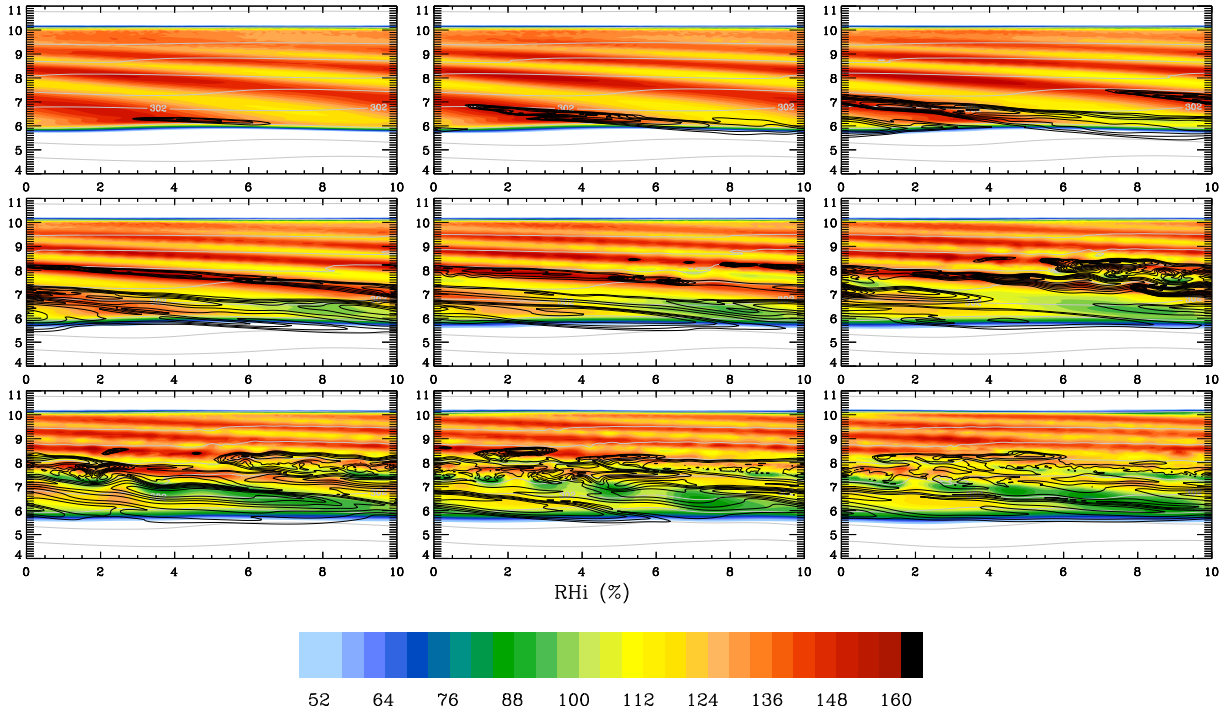

Fig. 3: Evolution of the moisture field due to the dynamical impact, starting at $t = 360$ min in time intervals of 36 min (upper panel: 360/396/432 min; middle panel: 468/504/540 min; lower panel: 576/612/648 min). Black lines indicate ice crystal number concentration of the formed cirrus clouds, grey lines indicate potential temperature.

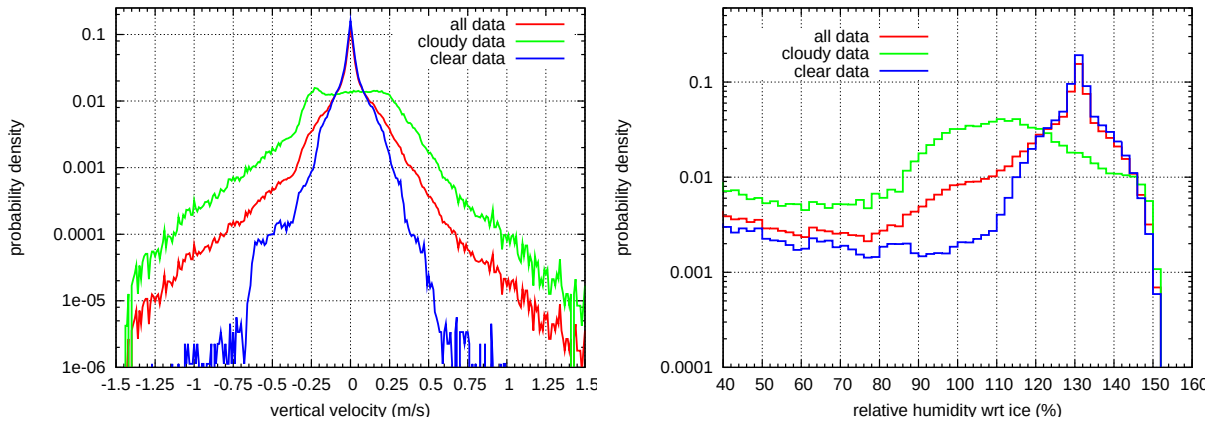

Fig. 4: Statistics of vertical velocity (left) and relative humidity wrt ice (right) inside the vertical layer $4 \leq z \leq 10.5$ km for all data (red), cloudy data (green) and clear air data (blue). A data point is labeled as cloudy if the ice crystal number density is larger than $0.1\mathrm{L}^{-1}$.

established in the upper altitude range beneath the critical level. However, the wave component (vertical velocities in the range $-0.25 \leq w \leq 0.25$) can be seen clearly (especially in the cloudy data), the long tails of the distribution are characteristic of turbulence. The relative humidity distributions are dominated by the initial values ($RHi = 130\%$), but the distributions are broaden by the vertical updrafts. The characteristic cut-off at $RHi \sim 150\%$ rep-

resents the homogeneous nucleation thresholds. For the cloudy data, high relative humidity values are relaxed to saturation, because ice crystals act as a strong sink for supersaturation. However, vertical velocity variations still present in the supersaturation layer, can modify this process leading to a broad maximum of relative humidity in the range $100 \leq RHi \leq 130\%$. This interpretation is corroborated by the vertical velocity distribution inside cirrus clouds (see fig. 4, left) indicating considerable updraft contributions leading to deviations of relative humidity from saturation.

Noteworthy, the vertical velocity distributions appear similar to the distributions of temperature fluctuations found by Gierens et al. (2007). This also supports our conjecture that variations in temperature/vertical velocity found in in situ measurements may originate from vertically propagating and dissipating waves.

5 CONCLUSIONS AND FUTURE WORK

We investigated the impact of turbulence formed by a dissipating wave near a critical level on the formation and evolution of cirrus clouds, using an idealized 2D setup with a prescribed wave length and amplitude. The vertically propagating wave and turbulence resulting from the wave breaking induce vertical updrafts which can trigger ice crystal formation; whereupon cirrus clouds can form nearby the critical level. These processes can be important for cirrus cloud formation in the natural atmosphere over mountainous terrain. Furthermore, inside cirrus clouds, the vertical velocity variations (resulting from wave and turbulence) broaden the relative humidity distribution; i.e., the relaxation to saturation is disturbed, whereupon higher relative humidities inside cirrus are possible.

The formation of ice crystals in the updraft regions of wave- and/or turbulent motions depend on the wave length and amplitude as well as on the environmental temperature and humidity. Herein, we only begun investigating the impact of the environment on the resulting cirrus. Our preliminary results indicate that initial supersaturation has a strong impact on the subsequent cloud evolution. For a drier supersaturated layer, the vertically propagating wave can only marginally trigger the ice formation, while the wave dissipating via turbulence can later induce much stronger updrafts leading to higher ice crystal number densities and, at later time, to longer life time of cirrus. Colder temperature may have a similar impact. Finally, it should be noted that the latent heat release from growing/evaporating ice crystals can modify the stability, thus changing the environment for the propagating waves. A thorough study of the sensitivity of cirrus evolution to the environmental conditions is a subject of the future work.

ACKNOWLEDGMENTS:
This work was partly supported by the European Commission within the framework of the Marie Curie Fellowship “Impact of mesoscale dynamics and aerosols on the life cycle of cirrus clouds” (IMDALCC). The numerical simulations were carried out at the European Centre for Medium–Range Weather Forecasts (special project “Ice supersaturation and cirrus clouds”).

REFERENCES

Booker, J. R. and F. P. Bretherton, 1967: The critical layer for internal gravity waves in a shear flow. Jour. Fluid Mech., 27, 513–539.

Chen T., W. Rossow, Y.Zhang, 2000: Radiative effects of cloud-type variations. J. Climate, 13, 264–286.

Clark T. L. and R. D. Farley, 1984: Severe downslope windstorm calculations in two and three spatial dimensions using anelastic interactive grid nesting: A possible mechanism for gustiness. J. Atmos. Sci., 41, 329–350.

DeMott, P. D. Cziczo, A. Prenni, D. Murphy, S. Kreidenweis, D. Thomson, R. Borys,

D. Rogers , 2003: Measurements of the concentration and composition of nuclei for cirrus formation. Proc. Nat. Acad. Sciences, 100, 14655–14660.

Fusina, F., P. Spichtinger, U. Lohmann, 2007: The impact of ice supersaturated regions and thin cirrus clouds on radiation. J. Geophys. Res., 112, D24S14, doi:10.1029/2007JD008449.

Gary. B. L., 2006: Mesoscale temperature fluctuations in the stratosphere, Atmos. Chem. Phys., 6, 4577–4589.

Gayet, J.-F., J. Ovarlez, V. Shcherbakov, J. Ström, U. Schumann, A. Minikin, F. Auriol and A. Petzold, Cirrus cloud microphysical and optical properties at southern and northern midlatitudes during the INCA experiment, J. Geophys. Res., 109, 2004.

Gierens, K., R. Kohlhepp, N. Dotzek, H. G. Smit, 2007: Instantaneous fluctuations of temperature and moisture in the upper troposphere and tropopause region. Part 1: Probability densities and their variability. Met. Z., 16, 221–231.

Grabowski, W.W. and P.K. Smolarkiewicz, 2002. A multiscale model for meteorological research. Mon. Weather Rev., 130, 939–956.

Grubisic, V. and P.K. Smolarkiewicz, 1997: The Effect of Critical Levels on 3D Orographic Flows: Linear Regime. J. Atmos. Sci., 54, 1943–1960.

Haag W. and B. Kärcher, 2004: The impact of aerosols and gravity waves on cirrus clouds at midlatitudes. J. Geophys. Res., 109, D12202.

Heymsfield, A. and J. Iaquinta, 2000: Cirrus crystal terminal velocities. J. Atmos. Sci., 57, 916–938.

Hoyle, C., B. Luo, T. Peter, 2005: The Origin of High Ice Crystal Number Densities in Cirrus Clouds. J. Atmos. Sci., 62, 2568–2579.

IPCC, 2007: Climate Change 2007: The Physical Science Basis. Contribution of Working Group I to the Fourth Assessment Report of the Intergovernmental Panel on Climate Change [Solomon, S., D. Qin, M. Manning, Z. Chen, M. Marquis, K.B. Averyt, M. Tignor and H.L. Miller (eds.)]. Cambridge University Press, Cambridge, United Kingdom and New York, NY, USA, 996 pp.

Kajikawa, M. and A. Heymsfield, 1989: Aggregation of ice crystals. J. Atmos. Sci., 46, 3108–3121.

Kärcher, B. and U. Lohmann, 2002: A Parameterization of cirrus cloud formation: Homogeneous freezing of supercooled aerosols. J. Geophys. Res., 107, 4010.

Kärcher, B., and J. Ström, The roles of dynamical variability and aerosols in cirrus cloud formation, Atmos. Chem. Phys., 3, 823–838, 2003.

Kärcher, B., J. Hendricks and U. Lohmann, 2006: Physically based parameterization of cirrus cloud formation for use in global atmospheric models J. Geophys. Res. , 111, D01205.

Koenig, L., 1971: Numerical modeling of ice deposition. J. Atmos. Sci., 28, 226–237.

Koop, T., B. Luo, A. Tsias, T. Peter, 2000: Water activity as the determinant for homogeneous ice nucleation in aqueous solutions. Nature 406, 611–614.

Krämer, M., 2008, pers. comm.

Prusa J.M., P.K. Smolarkiewicz, A.A. Wyszogrodzki, 2008: EULAG, a Computational Model for Multiscale Flows. Comput. Fluids; in press, doi:10.1016/j.compfluid.2007.12.001

Schlicht, S., P. Spichtinger, H. Vössing, C. Schiller, P. Konopka and M. Krämer, 2006:

A Cirrus Cloud Case Study in Frontal Systems over Norway using the Model EULAG. Geophysical Research Abstracts 8, 10535 (EGU General Assembly, Vienna).

Smith, S. and P. Jonas, 1996: Observations of turbulence in cirrus clouds. Atmos. Res., 43,, 1–29.

Smolarkiewicz P.K., 2006: Multidimensional Positive Definite Advection Transport Algorithm (MPDATA): An Overview. Int. J. Numer. Meth. Fluids, 50, 1123–1144.

Smolarkiewicz, P. and Margolin, L., 1997: On forward–in–time differencing for fluids: an Eulerian/Semi–Lagrangian non–hydrostatic model for stratified flows. Atmosphere–Oceans, 35, 127–152.

Smolarkiewicz, P., L. Margolin, A. Wyszogrodzki, 2001: A class of nonhydrostatic global models. J. Atmos. Sci., 58, 349–364.

Spichtinger, P. and K. Gierens, 2008a: Modelling Cirrus Clouds. Part 1: Model description and validation. Atmos. Chem. Phys. Diss., 8, 601–686.

Spichtinger, P. and K. Gierens: Modelling Cirrus Clouds. Part 2: Competition of different nucleation mechanisms. Atmos. Chem. Phys. Diss., accepted.

Vali, G, 1985: Nucleation terminology. J. Aerosol Sci., 16, 575–576.

Worthington, R.M., 1999: Tropopausal turbulence caused by the breaking of mountain waves. Jour. Atmos. Solar Terr. Phys., 59, 1543–1547.

Worthington, R. M. and L. Thomas, 1996: Radar measurements of critical–layer absorption in mountain waves. Quart. Jour. Roy. Meteorol. Soc., 122, 1263–1282.